

A Simple Electrochemical Immunosensor for Highly Sensitive Detection of Aflatoxin B₁ Based on Gold Nanoparticle Decorated Carboxylated Graphene Oxide

Ling Shi^{1,2}, Zefeng Wang^{1,2,*}, Na Wu^{1,2}, Xianlan Chen^{1,2}, Guangming Yang^{1,2,*}, Wei Liu^{1,2,*}

¹ School of science, Honghe University, mengzi, Yunnan 661199, PR China

² Key Laboratory of Natural Pharmaceutical & Chemical Biology of Yunnan Province, Mengzi, Yunnan 661199, PR China

*E-mail: wangzefeng841006@163.com, yangguangmingbs@126.com, liuwei4728@126.com

Received: 4 October 2019 / Accepted: 2 December 2019 / Published: 31 December 2019

In this work, polycrystalline gold nanoparticles decorated carboxylated graphene oxide (Au-COOH-GO) nanohybrids have been prepared and were used to fabricate electrochemical immunosensor for detecting of aflatoxin B₁ (AFB₁). The obtained Au-COOH-GO nanohybrids are characterized by transmission electron microscope (TEM), X-ray photoelectron spectroscopy (XPS) and UV-vis absorption spectra. Each step of the immunoelectrode design is evaluated using cyclic voltammetry (CV) and electrochemical impedance spectroscopy (EIS). The surface reaction mechanism of AFB₁ on Au-COOH-GO nanohybrids also has been investigated. The concentration and incubation time of antibody, pH, and immunoreaction time are optimized by square wave voltammogram (SWV). Under the optimal conditions, the detection limit of AFB₁ is 0.05 ng mL⁻¹ (S/N=3) with a linear AFB₁ concentration range of 0.05 to 25 ng mL⁻¹. The fabricated immunosensor shows a good reproducibility, stability, and selectivity and can successfully detect AFB₁ in real rice sample.

Keywords: Gold nanoparticles; Carboxylated graphene oxide; Aflatoxin B₁; Electrochemical immunosensor

1. INTRODUCTION

Aflatoxin B₁ (AFB₁) is a highly toxic difuranocoumarin derivative produced mainly by *Aspergillus flavus* and *A. parasiticus* [1]. AFB₁ is considered as one of the most potent teratogenicity, mutagenicity, carcinogenicity and toxicity to human and animal health [2]. The AFB₁ usually appears widely in variety of agricultural and sideline products. For example, rice, wheat, peanut, maize, nuts, soybean, fruits and vegetable [3]. The State Administration of Quality Supervision and Administration of the People's Republic of China proposes that the regulatory limit is 20 ng mL⁻¹ of AFB₁ in foodstuff

[1]. Therefore, developing reliable, selective, sensitive and accurate analytical methods to detect of AFB₁ is of great importance.

In recent years, a variety of analytical techniques have been proposed for AFB₁ determination. Such as, the liquid chromatography/tandem mass spectrometry (LC/MS) [4], the high performance liquid chromatography (HPLC) [5], enzyme-linked immunosorbent assay (ELISA) [6], electrochemiluminescence (ECL) [1], surface plasmon resonance (SPR) [7], and many immunoassay methods [1, 2, 8]. Although these above methods can successfully detect AFB₁, some methods are relatively complex, time-consuming, and need expensive instruments or skillful operators. Biosensing methods are alternatives for detection of aflatoxins due to its simple, high sensitivity and specificity, cost-effectiveness, and portable detection. Electrochemical immunoassay exhibits high sensitivity and high specificity for the detection of pesticide residues, diseases, and environmental pollutants.

With the development of sensing technology, the design of biosensors with good performance has become more fascinating. It is very critical that functional modification of the electrode surface. That will be benefit for immobilization of biomolecules which could affect the sensitivity and the selectivity of sensor. Because the introduction of multifunctional nanomaterials can help to achieve a direct wiring of electrode with the biomolecules [9]. Graphene has been greatly applied in developing electrochemical biosensors due to its fast electron-transfer kinetics, large surface area and high electrical conductivity [10]. Carboxylated graphene oxide (COOH-GO) is a derivative of graphene oxide (GO). The presence of abundant oxygen-containing groups at the edges/surface of COOH-GO, which allows COOH-GO possess excellent solubility and strong conductivity. Furthermore, a large of functional groups is benefit for loading metal nanoparticles and immobilizing biomolecules, and further improves the electron transfer rate [11]. In addition, the gold nanoparticles (Au NPs) have recently attracted enormous research attention in biosensor due to its excellent biocompatibility, catalytic, unique photophysical properties. More importantly, the properties of Au nanoparticles (NPs) can be affected by their size, shape and surrounding chemical environment [12, 13]. In other words, the electrochemical performance of Au-based nanomaterials depends on the shapes of Au NPs to a great extent. Furthermore, incorporation of Au NPs and other nanomaterials can simultaneously enhance charge transfer ability and are beneficial to the improvement of electrochemical performance.

In this paper, polycrystalline Au NPs decorated COOH-GO (Au-COOH-GO) nanohybrids were prepared. The introduction of polycrystalline Au NPs can effectively inhibit the aggregation of COOH-GO nanosheets, COOH-GO can disperse of Au NPs to fabricate Au NPs decorated COOH-GO nanohybrids. Meantime, the large surface areas and electroactive sites are benefit for immobilizing biomolecules. Here, a label-free immunosensor based on Au-COOH-GO nanohybrids has been developed for simple and sensitive determination of AFB₁. The excellent performance of Au-COOH-GO nanohybrids is benefit for immobilizing Anti-AFB₁ antibodies. The fabricated immunosensor reveal good sensitivity and selectivity for the detection of AFB₁, the proposed sensor can be applied in real samples.

2. EXPERIMENTAL

2.1 Materials

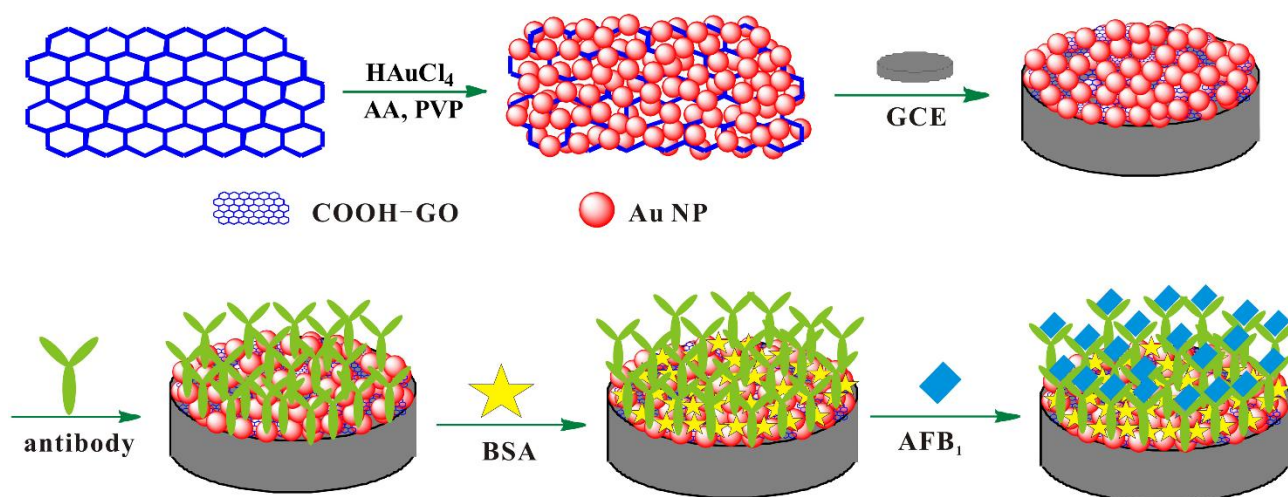
Carboxylated graphene oxide dispersion solution is obtained from Nanjing Jcnano Technology Co., Ltd (China). HAuCl_4 (99.99%, wt.%), AFB_1 , mouse anti- AFB_1 monoclonal antibody, bovine serum albumin (BSA) are obtained from Shanghai Eybridge Chemical Technology Co., Ltd. Polyvinylpyrrolidone (PVP, $M=55000 \text{ g mol}^{-1}$), ascorbic acid and other reagents are analytical-grade reagents. The phosphate buffer solution is prepared using NaH_2PO_4 and Na_2HPO_4 . Ultra-pure water which is obtained from a Milli-Q water purifying system is used for preparation of all aqueous solutions.

2.2 Preparing of Au nanoparticles decorated COOH-GO nanohybrids

PVP (35 mg) and ascorbic acid (60 mg) are ultrasonically dispersed in 4.0 mL ultra-pure water. Then 2 mL COOH-GO dispersion (0.5 mg mL^{-1}) is added into the above solutions. The obtained mixture solution is reacted 10 min at $90 \text{ }^\circ\text{C}$ under magnetic stirring. Then, HAuCl_4 solution (1 mL, 3 mM) is dropwise added to the stirred above solutions, and the reaction mixture is stirred for 3 h until the Au precursor is reduced completely. The resulting Au-COOH-GO nanohybrids are collected by centrifugation, completely washed with ethanol and resuspended in ultrapure water for further use. The obtained sample is defined as sample 1.

2.3 Fabrication of the immunosensor and measurement procedure

The bare glassy carbon electrode (GCE, 3 mm diameter) is polished with 1.0, 0.3, 0.05 μm alumina slurry in sequence, then washed sequentially with ethanol and ultrapure water by ultrasonic and dried in air. The sample 1 is used to conduct electrochemical experiments. The 7 μL of Au-COOH-GO solution is dropped on the GCE surface. The electrode is incubated in an 150 $\mu\text{g/mL}$ AFB_1 antibody solution for 40 min at $37 \text{ }^\circ\text{C}$ after drying in the air, it is rinsed thoroughly with PBS (pH=7.0) solution to remove the unstable AFB_1 antibody on the GCE surface. And then the obtained electrode is incubated in 0.2 % BSA solution for 40 min at $37 \text{ }^\circ\text{C}$ in order to block the unspecified active sites. Finally, the electrode is incubated into AFB_1 antigen solution for about 30 min at $37 \text{ }^\circ\text{C}$, then rinsed with PBS (pH 7.0) to remove the physically adsorbed AFB_1 antigen molecules, stored at $4 \text{ }^\circ\text{C}$. The preparation of Au-COOH-GO nanohybrids and the fabricated strategy of electrochemical immunosensor towards AFB_1 are depicted in Scheme 1.



Scheme 1. Schematic representation of the preparation process of the immunosensor.

2.4 Characterization

UV-vis absorption spectra are carried out on a Puxi TU-1900 spectrophotometer. ESCALAB 250XI X-ray photoelectron spectroscopy (XPS) is used to characterize composition of nanomaterials. The morphology analysis is performed on JEM-2100 transmission electron microscope (JEOL Ltd.). Cyclic voltammogram (CV) and square wave voltammogram (SWV) experiments are performed using CHI 660E electrochemical analyzer (CHI, Shanghai) with standard three-electrode system: working glassy carbon electrode (GCE, 3 mm diameter) versus saturated Ag/AgCl reference electrode and a platinum wire as counter electrode. For the electrochemical measurement, antigen and antibody with different concentrations are dissolved in 0.2 M PBS (pH 7.0). The CV, SWV and the impedance experiments are conducted in PBS solution containing 1.0 mM $\text{Fe}(\text{CN})_6^{3-/4-}$ and 0.1 M KCl. The peak current change (ΔI) is used to evaluate the electrode-to-electrode variation: $\Delta I = I_i - I_0$, where I_i and I_0 are the current response values measured in blank solution and in AFB_1 solution.

2.5 Sample preparation

The sample is obtained according to our reported method previously [14]. The rice is purchased from local market. Ground rice (10 g) is ultrasonic extracted with 50 mL of methanol-water (1:1, v/v) with 30 min. The extract is collected by centrifugating. The obtained extraction is diluted 1:5 with 0.2 M PBS and spiked with different concentration of AFB_1 (5.0, 10.0, 15.0 ng mL^{-1}). Finally, the spiked extracts are incubated for 30 min at 37 °C, and the SWV responses are recorded as previously described

3. RESULT AND DISCUSSION

3.1 Synthesis and characterization of Au-COOH-GO nanohybrids

The UV absorption spectrum of obtained sample is shown in Figure 1. The COOH-GO shows an obvious peak at 230 nm and a shoulder peak about 300 nm. This corresponds to π - π^* and n - π^* transitions of aromatic C=C and C=O bonds, respectively [15]. After the Au NPs are decorated onto the surface COOH-GO, the absorption peak of COOH-GO is redshifted 2 nm to 232 nm, that maybe due to the interactions between COOH-GO and Au NPs. Also a broad peak at 515 nm assigned to the surface plasma adsorption band of Au NPs [16].

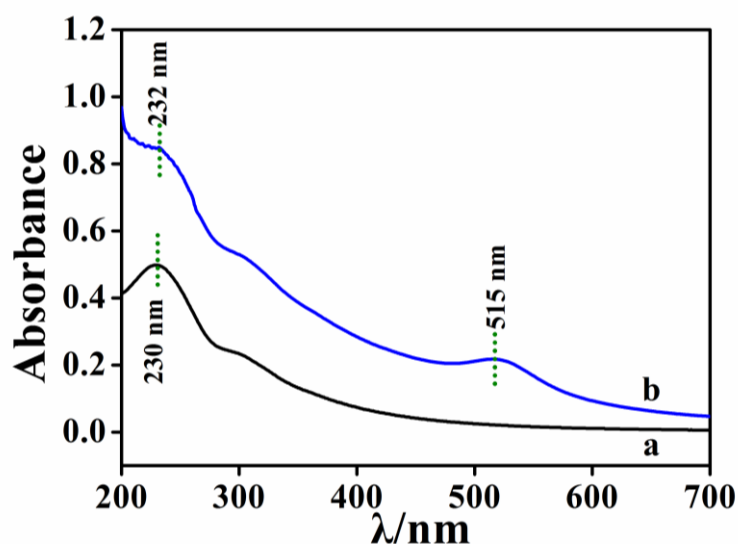


Figure 1. UV-vis spectra of (a) COOH-GO, and (b) Au-COOH-GO nanocatalysts.

Figure 2A shows the XPS of Au-COOH-GO nanocatalysts. The dominant XPS peaks at 284.65 eV, 532.64 eV, 398.97 eV, and 83.76 eV come from C1s, O1s, N1s, and Au4f, respectively. Figure 2B shows high resolution XPS spectra of C1s core level of Au-COOH-GO nanocatalysts which is consisted of three main peaks. The binding energy at 284.8 eV is attributed to the C-C of aromatic ring [17]. The peak at 287.4 eV is attributed to keto group (C=O) of carbonyl and carboxyl groups. The presence of C-N bond at 285.8 eV which further confirm the successfully doping of N into GO [18]. As shown in Figure 2C, the core spectra of O1s displays two peaks at about 531.1 eV and 532.4 eV corresponded to the C=O and C-O. Figure 2D shows high resolution Au4f spectra. There are two peaks at 83.8 eV and 87.5 eV are contributed to $4f_{7/2}$ and $4f_{5/2}$ of the metallic Au (0) state, respectively [19].

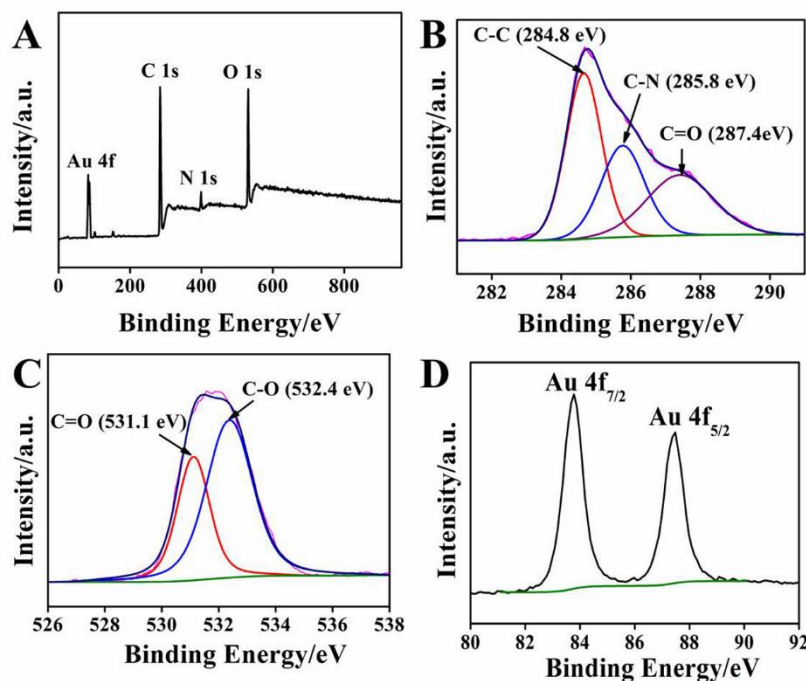


Figure 2. Survey of Au-COOH-GO nanocatalysts (A), and high-resolution (B) C1s, (C) O1s, and (D) Au4f XPS spectra of Au-COOH-GO nanocatalysts.

Interestingly, we found that the metal ion concentration can effectively affect the size and shape of Au NPs in Au-COOH-GO nanocatalysts. As shown in Figure 3, the COOH-GO shows a lamellar and transparent film shape. When the concentration of HAuCl_4 is 3.0 mM, we found that the irregular shaped Au NPs evenly distributed on the surface of COOH-GO sheets with minimal agglomeration (Figure 3A). The irregular shaped Au NPs are comprised of hexagonal, pentagonal and spherical shapes. The average size of Au NPs is about 19.0 nm. The results further show formation of polycrystalline Au NPs in sample of Au-COOH-GO nanocatalysts. When the concentration of HAuCl_4 is further increased to 4.0 mM, the TEM image (Figure 3B) shows that the shapes of Au NPs are relatively complex and the size of Au NPs are very uneven. That maybe due to the initially formed Au NPs are not stabilized effectively, and excess HAuCl_4 are liable to accumulate on the initially formed Au NPs. That will result secondary growth of Au NPs and cause the average particle size of Au NPs increase. Furthermore, the reaction rate is accelerated with the increase of concentration and formed very smaller sized Au NPs in the very beginning, which will resulting in the formation of uneven Au NPs decorated onto the COOH-GO. Then lead to form various shapes of Au NPs decorated onto the COOH-GO [20].

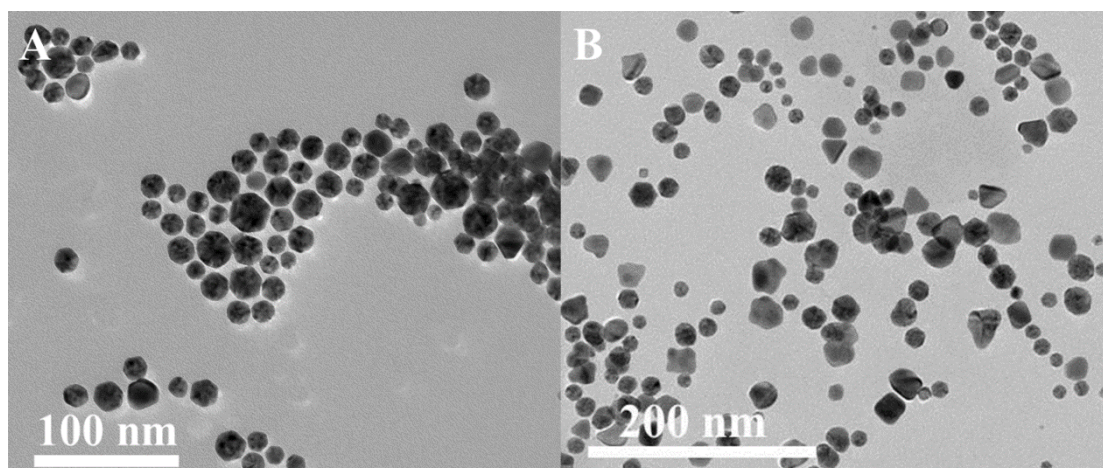


Figure 3. TEM images of Au-COOH-GO nanocatalysts: (A) 1 mL of an aqueous 3.0 mM H_{AuCl}₄ solution; (B) 1.0 mL of an aqueous 4.0 mM H_{AuCl}₄ solution.

3.2 Characterization of the immunosensor fabrication

In order to investigate the interface features of surface-modified electrodes, CV and EIS are used as effective methods to discuss the interface features of immunosensors [21, 22]. Figure 4A shows the CVs of Au-COOH-GO/GCE (a), anti-AFB₁/Au-COOH-GO/GCE (b), BSA/anti-AFB₁/Au-COOH-GO/GCE (c), AFB₁/BSA/anti-AFB₁/Au-COOH-GO/GCE (d) in 0.2 M pH=7.0 PBS containing 1.0 mM [Fe(CN)₆]^{4-/3-} and 0.1 M KCl at a scan rate of 25 mV s⁻¹. The Au-COOH-GO/GCE shows two prominent peaks with ΔE_p ($E_{pa}-E_{pc}$) value of 80 mV. The I_{pa} and I_{pc} are 3.52 μ A and -2.81 μ A (curve a), respectively. After the antibodies are incubated on Au-COOH-GO/GCE, the ΔE_p value increased to 108 mV, the value I_{pa} and I_{pc} decreases to 2.97 μ A and -2.6 μ A, respectively (curve b). That mainly due to the antibody blocks the active sites and further blocking the electron transfer between [Fe(CN)₆]^{3-/4-} and the electrode. The peak current further decreases when BSA is immobilized on the electrode surface (curve c). This phenomenon proves that the BSA has blocked the unrecognized active sites. Lastly, the peak current further decreased after AFB₁ antigens are incubated (curve d). The results reveal that antibody-antigen immunocomplexes have formed successfully, which hinder the diffusion of [Fe(CN)₆]^{3-/4-} toward the electrode surface [23].

EIS is used to investigate the resistance occurring in the charge transfer mechanism within the interface of the electrode and the electrolyte solution. As show in Figure 4B, the Au-COOH-GO/GCE reveals a straight line (curve a), proving that the electron-transfer process is very fast in electrochemical process. The resistance is increased after the antibodies are incubated which implies a lower electron-transfer rate at the electrode interface (curve b). The semicircle diameter increases obviously when BSA is incubated (curve c). The result illustrates the BSA is successfully blocked the active sites of nonspecific adsorption. The semicircle diameter is remarkably increased when formation of antibody-antigen immunocomplexes (curve d) [24]. The all results show that the electrochemical immunosensor of AFB₁ is successfully fabricated.

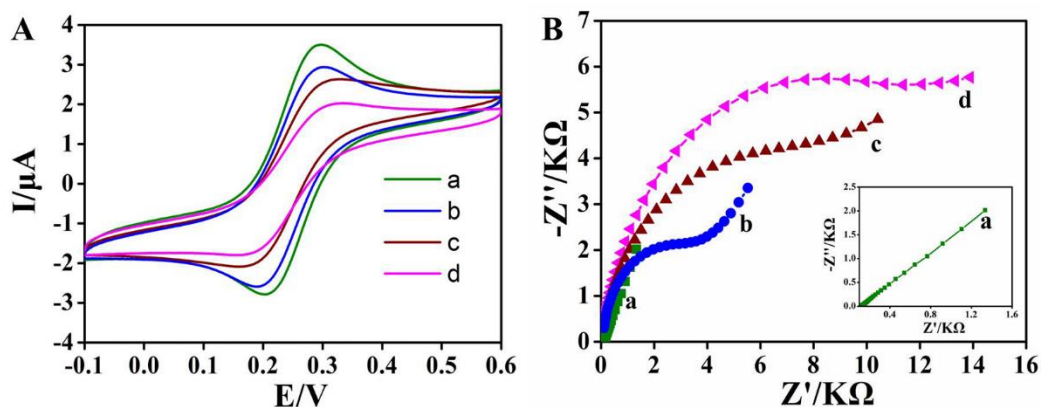


Figure 4. Cyclic voltammograms (A) and EIS spectrums (B) of Au-COOH-GO/GCE (curve a), anti-AFB₁/Au-COOH-GO/GCE (curve b), BSA/anti-AFB₁/Au-COOH-GO/GCE (curve c), AFB₁/BSA/anti-AFB₁/Au-COOH-GO/GCE (curve d). All measurements were processed in 0.2 M pH=7.0 PBS containing 1.0 mM [Fe(CN)₆]^{4-/3-} and 0.1 M KCl. The concentration of AFB₁ is 10 ng mL⁻¹.

3.3 Mechanism of the electrochemical process on the immunosensor

The electrochemical reaction mechanism of AFB₁ on immunosensor is investigated using CV at different scan rates. As shown in Figure 5A, the redox peak currents are increased linearly with the increasing of scan rate from 15 to 100 mV s⁻¹. The linear regression equations between peak currents and square root of scan rates can be obtained from Figure 5B. The linear regression equations are as follows: $I_{pa} (\mu A) = 16.80 v^{1/2} - 0.11$ ($R^2=0.9940$) and $I_{pc} (\mu A) = -16.70 v^{1/2} + 0.33$ ($R^2=0.9955$). The results revealing that the electrochemical reaction of AFB₁ on AFB₁/BSA/anti-AFB₁/Au-COOH-GO immunosensor is diffusion controlled process [25, 26]. In addition, Figure 5A also shows that the oxidation peak potentials shifted in the positive direction and the reduction peak potentials shifted in the negative direction with increasing of scan rate. Figure 5C shows the plots of anode and cathode peak potential against $\lg v$, respectively. The linear equations are: $E_{pa} (V) = 0.107 \lg v (V/s) + 0.532$ ($R^2=0.9778$) and $E_{pc} (V) = -0.075 \lg v (V/s) + 0.029$ ($R^2=0.9646$), respectively. Based on the Laviron's theory [27], the slopes can be used to calculate the transfer coefficient (α) and charge electron transfer rate constant (k_s) according to the following relation:

$$E_{pa} = E^{0'} + \frac{2.303RT}{(1-\alpha)nF} \lg v \quad E_{pc} = E^{0'} - \frac{2.303RT}{\alpha nF} \lg v$$

$$\lg k_s = \alpha \lg(1-\alpha) + (1-\alpha) \lg \alpha - \lg \frac{RT}{nFv} - \alpha(1-\alpha) \frac{nF\Delta E_p}{2.3RT}$$

where $E^{0'}$ is the formal standard potential, n is the transferred electron number, R is gas constant, F is Faraday constant, T is thermodynamic temperature, ΔE_p is the peak-to-peak potential separation. According to the Laviron's theory, α is 0.59, n is 1.0, and k_s is 0.09 s⁻¹.

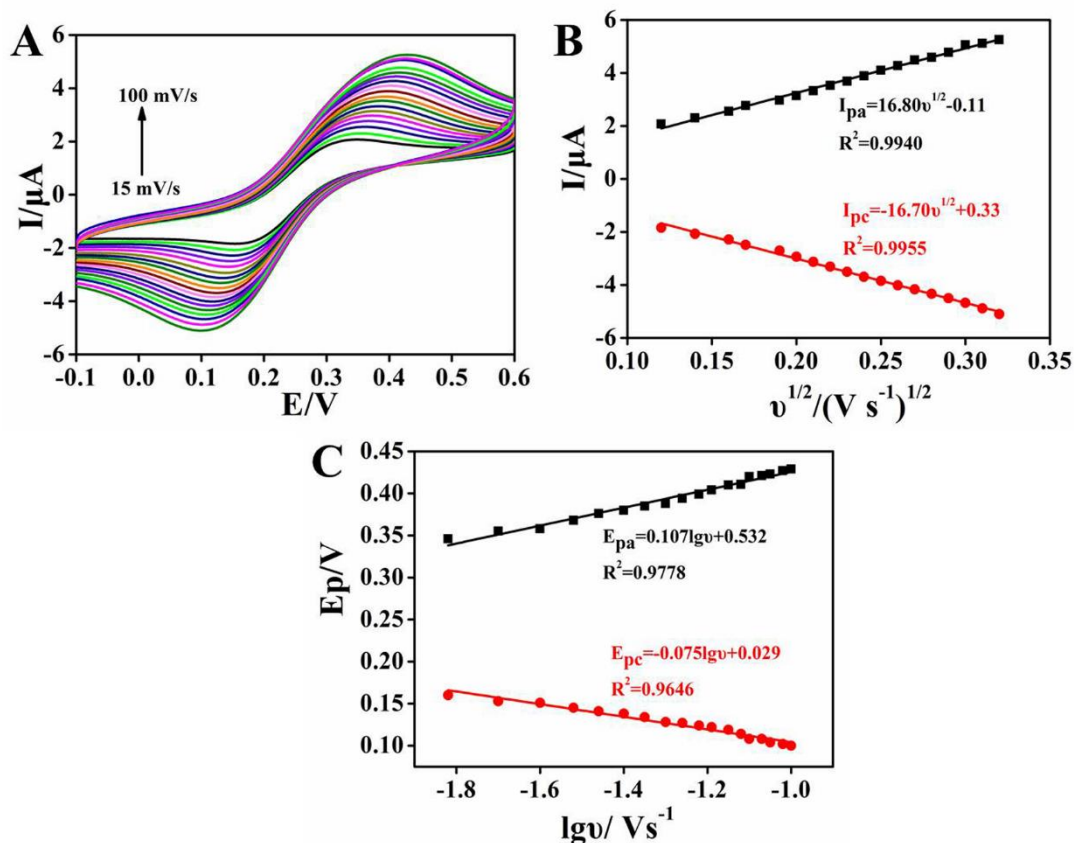


Figure 5. (A) CV of AFB₁/BSA/anti-AFB₁/Au-COOH-GO/GCE immunosensor at different scan rates in 0.2 M pH=7.0 PBS containing 1.0 mM [Fe(CN)₆]^{4-/3-} and 0.1 M KCl. (B) The relationship of peak current vs square root of scan rates. (C) The relationship of peak potential vs logarithm of scan rates.

3.4 Optimization of immunization conditions

In order to optimize the immunoassay conditions, the effects of the concentration, incubation time of antibody, pH, and immunoreaction time are investigated. Figure 6A shows the effect of concentration of the antibody on the performance of immunosensor. When the concentration of antibody increased from 25 $\mu\text{g mL}^{-1}$ to 200 $\mu\text{g mL}^{-1}$, the peak current changes significantly increased with the increasing antibody concentration till the peak current reached a plateau at 150 $\mu\text{g mL}^{-1}$. That maybe due to the mass of anti-AFB₁ immobilized on sensor surface is almost saturated [28]. Thus, 150 $\mu\text{g mL}^{-1}$ is chosen in subsequent experiments.

Solution pH is also play an important effect in the performance of the immunosensor. The influence of pH is investigated in range of pH range 5.0-8.0. As shown in Figure 6B, the maximum current change is obtained at pH 7.0. This phenomenon can be due to the denaturation of the biological activity of antibodies/antigens in acidic or alkaline solutions [28, 29]. So, the optimal pH is 7.0.

The effect of incubation time of anti-AFB₁ is investigated in the range from 20 to 60 min. From the results shown in Figure 6C, the peak current change increased from 20 min to 40 min, and decreased from 40 min to 60 min. Thus, 40 min is selected as the optimal incubation time for anti-AFB₁.

The incubation time is also investigated. As shown in Figure 6D, the peak current change increased and reached maximum at 30 min when increasing reaction time from 10 to 30 min. and the peak current change is tended to reach a saturation value when increasing the reaction time. This phenomenon indicating that the balance of the antigen-antibody reaction is achieved at 30 min. Therefore, 30 min is selected as optimal immune reaction time.

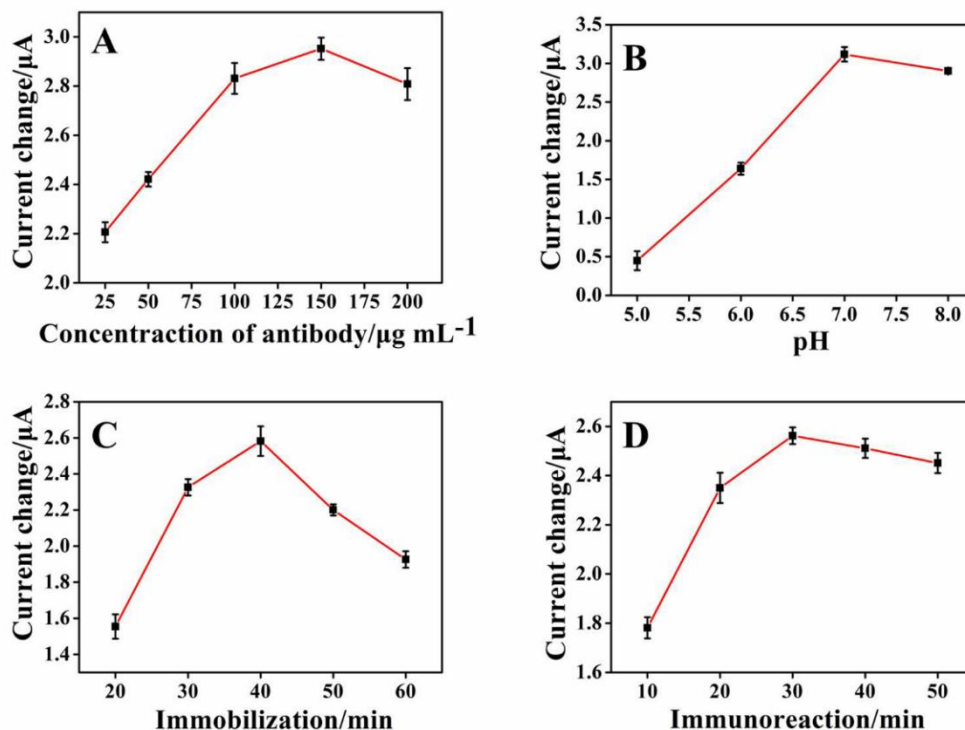


Figure 6. Effects of antibody concentration (A), pH (B), antibody immobilization time (C) and immunoreaction time (D) on peak current of immunosensor. The concentration of antigen is 10 ng mL^{-1} .

3.5 Electrochemical detection of AFB_1

The SWV measurement is used to detected AFB_1 standard solutions with different concentrations under optimal conditions. As shown in Figure 7A, the peak current values gradually decreased with the increasing of AFB_1 concentration from 0 to 25 ng mL^{-1} . The peak current is proportional to the concentration of AFB_1 range from 0.05 to 25 ng mL^{-1} with a detection limit of 0.05 ng mL^{-1} ($S/N=3$). The linear regression equations is $I=0.17C-6.965$ ($R^2=0.9937$). The analytical performance of the immunoassay has been compared with those of other AFB_1 immunoassays reported (Table 1). The comparative data suggested that the present sensor has a good immunity for the detection of AFB_1 .

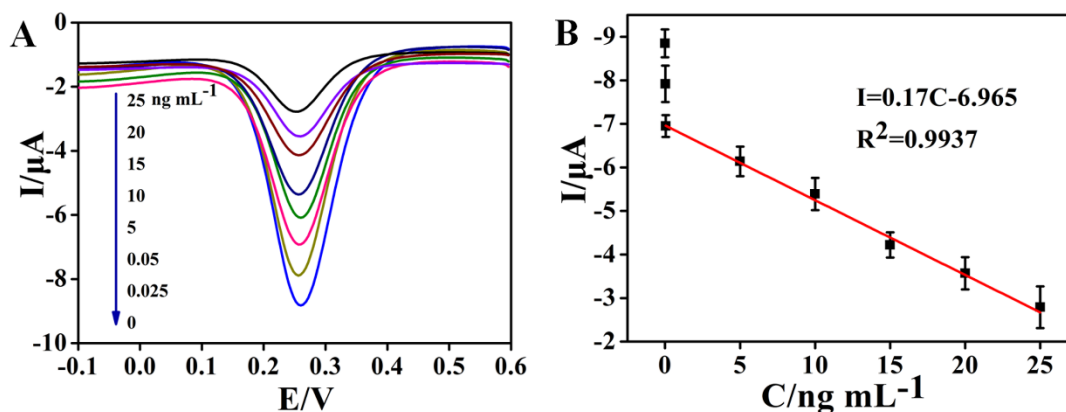


Figure 7. SWV responses of the immunosensor to different concentrations of AFB₁ (A). Calibration curve of the immunosensor to different concentrations of AFB₁ (B).

Table 1. Comparison with other reported methods for the determination of AFB₁.

Immunosensors	Linear range (ng mL ⁻¹)	Detection limit (ng mL ⁻¹)	References
BSA/anti-AFB ₁ /rGO/ITO	0.125-1.5	0.12	[30]
BSA/anti-AFB ₁ /Ni-ITO	0.05-1	0.327	[31]
BSA-anti-AFB ₁ /Au NPs	0.5-10	0.1	[32]
BSA/anti-AFB ₁ /Au@rGO/ITO	0.1-12	0.10	[33]
AFB ₁ /BSA/anti-AFB ₁ /Au-COOH-GO	0.05-25	0.05	This work

3.6 Reproducibility, stability, and selectivity of immunosensor

The reproducibility of the immunosensor for AFB₁ is evaluated by prepared five modified working electrodes under the same conditions (Figure 8A). The results reveal that the relative standard deviation (RSD) of the AFB₁ measurements for five sensors is 2.25%, proving that the proposed immunosensor has good reproducibility. In addition, the stability of immunosensor is also studied, the fabricated immunosensor is stored in a refrigerator for four weeks at 4 °C. As shown in Figure 8B, the current still kept 94.6% of initial current value, revealing that the immunosensor possess good stability. Furthermore, the selectivity of the immunosensor also has been investigated to evaluate the specificity of immunosensors. The immunosensor is incubated with AFB₂, AFM₁, AFG₁ under the same condition. As can be seen from Figure 8C, the selected antigens are almost no interference for detection of AFB₁. The results show that the immunosensor possessed good selectivity for determination of AFB₁.

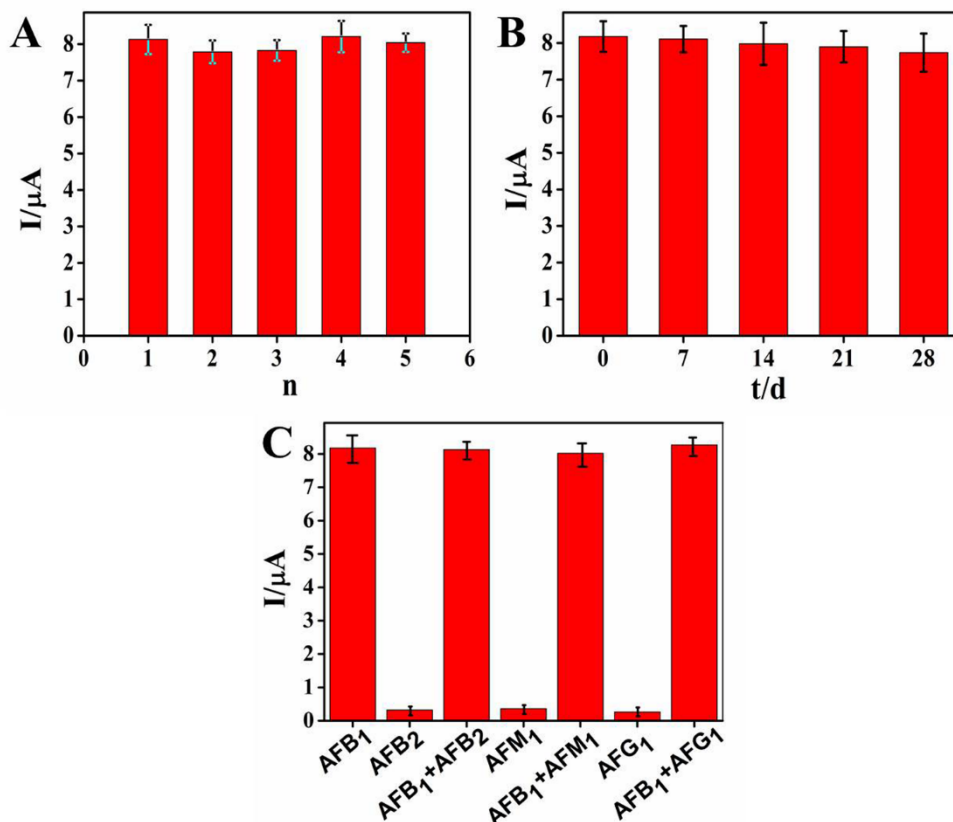


Figure 8. Amperometric change response of immunosensor to 5 different electrodes treated in the same way (A); the time stability study of the immunosensor (B), current responses of the immunosensor to AFB₁, AFB₂, AFB₁+ AFB₂, AFM₁, AFB₁+ AFM₁, AFG₁, AFB₁+ AFG₁ (C).

3.7 Detection of AFB₁ in rice samples

In order to demonstrate the reliability of this immunosensor, the standard addition method is used for the detection of AFB₁ in rice. As presented in Table 2, the recovery of rice samples ranged from 98.9% to 101.2%. The results indicating that the proposed method is acceptable for analyses of AFB₁ in spiked rice samples.

Table 2. Detection of the AFB₁ in rice samples with the proposed immunosensor.

Samples	Standard concentration (ng mL ⁻¹)	Found (ng mL ⁻¹)	Recovery (%)	RSD%
1	5.00	5.06	101.2	3.8
2	10.00	9.89	98.9	2.3
3	20.00	20.13	100.7	4.1

4. CONCLUSION

In this work, we developed an electrochemical immunosensor based on polycrystalline gold nanoparticles decorated carboxylated graphene oxide (Au-COOH-GO) for the detection of AFB₁. A lot

of functional groups, large specific surface area, excellent biocompatibility and electrochemical activity of Au-COOH-GO nanohybrids are benefit for immobilizing antibody, and further improves the electron transfer rate. The obtained Au-COOH-GO nanohybrids are characterized by TEM, XPS and UV-vis. The concentration and incubation time of antibody, pH, and immunoreaction time are optimized by SWV. Under the optimal conditions, the detection limit of AFB₁ is 0.05 ng mL⁻¹ (S/N=3) with a linear AFB₁ concentration range of 0.05 to 25 ng mL⁻¹. The fabricated immunosensor shows a good reproducibility, stability, and selectivity and can successfully detect AFB₁ in real rice sample. The results show that the proposed AFB₁ immunosensor is simple, sensitive, and fast, which opens up a new promising AFB₁ platform for other small molecules analysis.

ACKNOWLEDGMENTS

This work supported by the National Natural Science Foundation of China (Grand No. 21665008), the Scientific Research Fund Project of Honghe University (Grand No. XJ14Z02), Junior High School Academic and Reserve Program of Yunnan Province (Grand No. 2018HB005), the Yunnan education department of Scientific Research Foundation (Grand No. 2018JS478), the PhD Start-up Fund of Honghe University (Grand No. XJ16B04), Young Academic Reserve Program of Honghe University (Grand No. 2016HB0401).

References

1. Y. G. Wang, G. H. Zhao, X. J. Li, L. Liu, W. Cao and Q. Wei, *Biosensors Bioelectron.*, 101 (2018) 290.
2. J. H. Feng, Y. Y. Li, Z. Q. Gao, H. Lv, X. B. Zhang, Y. H. Dong, P. Wang, D. W. Fan and Q. Wei, *Sensors and Actuators B*, 270 (2018) 104.
3. T. Sergeyeva, D. Yarynka, E. Piletsk, R. Linnik, O. Zaporozhets, O. Brovko, S. Piletsky and A. El'skay, *Talanta*, 201 (2019) 204.
4. A. Ouakhssase, A. Chahid, H. Choubbane, A. Aitmazirt and E. A. Addi, *Heliyon*, 5 (2019) e01565.
5. C. Tacconi, M. Cucina, C. Zadra, G. Gigliotti and D. Pezzolla, *J. Environ. Chem. Eng.*, 7 (2019) 103046.
6. P. Vila-Donat, S. Marín, V. Sanchis and A. J. Ramos, *Anim. Feed Sci. Technol.*, 255 (2019) 114228.
7. W. B. Wu, Z. L. Zhu, B. Jie Li, Z. Q. Liu, L. L. Jia, L. M. Zuo, L. Chen, Z. T. Zhu, G. Z. Shan and S. Z. Luo, *Toxicon*, 146 (2018) 24.
8. Z. B. Abdallah, C. Grauby-Heywang, L. Beven, S. Cassagnere, F. Moroté, E. Maillard, H. Sghaier and T. C. Bouhacina, *Biochem. Eng. J.*, 150 (2019) 107262.
9. H. Wan, Q. Sun, H. Li, F. Sun, N. Hu and P. Wang, *Sensors Actuators B: Chem.*, 209 (2015) 336.
10. Y. Si and E. T. Samulski, *Nano Lett.*, 8 (2008) 1679.
11. X. F. Ma, Y. L. Wu, S. Devaramani, C. Z. Zhang, Q. X. Niu, M. Ibrahim, W. Q. Li, D. L. Shan and X. Q. Lu, *Talanta*, 178 (2018) 962.
12. S. H. Xu, T. Gao, X. Y. Feng, X. J. Fan, G. F. Liu, Y. N. Mao, X. J. Yu, J. H. Lin and X. L. Luo, *Biosensors Bioelectron.*, 97 (2017) 203.
13. T. Xiao, J. S. Huang, D. W. Wang, T. Meng and X. R. Yang, *Talanta*, 206 (2020) 120210.
14. L. Shi, Z. F. Wang, G. M. Yang, X. L. Chen, G. Z. Gou and W. Liu, *Electrochemistry*, 85 (2017) 384.
15. J. L. Wang, F. J. Trindade, C. B. d. Aquino, J. C. Pieretti, S. H. Domingues, R. A. Ando and P. H. C. Camargo, *Chem. Eur. J.*, 21 (2015) 9889.
16. F. X. Chen, G. Q. Xu and T. S. A. Hor, *Mater. Lett.*, 57 (2003) 3282.

17. D. O. Idisia, H. Alib, J. A. Okea, S. Sarmaa, S. J. Moloia, S. C. Raya, Wangc, H.T. , N. R. Janab, W. F. Pongd and A. M. Strydome, *Appl. Surf. Sci.*, 483 (2019) 106.
18. F. Y. Kong, L. Yao, R. F. Li, H. Y. Li, Z. X. Wang, W. X. Lv and W. Wang, *J. Alloys Compd.*, 797 (2019) 413.
19. Y. J. Gu, C. Ju, Y. J. Li, Z. Q. Shang, Y. D. Wu, Y. F. Jia and Y. J. Niu, *Biosensors Bioelectron.*, 66 (2015) 24.
20. S. Phukan, P. Bharali, A. K. Dasb and M. H. Rashid, *RSC Adv.*, 6 (2016) 49307.
21. A. Sharma, A. Kumar and R. Khan, *Synth. Met.*, 235 (2018) 136.
22. A. Sharma, A. Kumar and R. Khan, *Mater. Sci. Eng., C*, 76 (2017) 802.
23. S. B. Zhang, Y. M. Shen, G. Y. Shen, S. Wang, G. L. Shen and R. Q. Yu, *Anal. Biochem.*, 494 (2016) 10.
24. L. G. Chen, J. H. Jiang, G. L. Shen and R. Q. Yu, *Analytical Methods*, 7 (2013) 2354.
25. A. O. Idris, N. Mabubaab and O. A. Arotiba, *Anal. Methods*, 10 (2018) 5649.
26. P. Wang, F. B. Pei, E. H. Ma, Q. S. Yang, H. X. Yu, J. Liu, Y. Y. Li, Q. Liu, Y. H. Dong and H. J. Zhu, *Bioelectrochem.*, 131 (2020) 107352.
27. E. LAVIRON, *J. Electroanal. Chem.*, 101 (1979) 19.
28. P. D. Tam and C. X. Thang, *Mater. Sci. Eng., C*, 58 (2016) 953.
29. Z. Qiang, R. Yuan, Y. Q. Chai, Na Wang, Y. Zhuo, Y. Zhang and X. L. Li, *Electrochim. Acta*, 51 (2006) 3763.
30. S. Srivastava, V. Kumar, M. A. Ali, P. R. Solanki, A. Srivastava, G. Sumana, P. S. Saxena, A. G. Joshi and B. Malhotra, *Nanoscale*, 5 (2013) 3043.
31. P. Kalita, J. Singh, M. Kumar Singh, P. R. Solanki, G. Sumana and B. Malhotra, *Appl. Phys. Lett.*, 100 (2012) 093702.
32. Y. Liu, Z. Qin, X. Wu and H. Jiang, *Biochem. Eng. J.*, 32 (2006) 211.
33. S. Srivastava, S. Abraham, C. Singh, M. A. Ali, A. Srivastava, G. Sumanaa and B. D. Malhotr, *RSC Adv.*, 5 (2015) 5406.